Supplementary Information for

Increased probability of hot and dry weather extremes during the growing season threatens global crop yields

Matias Heino, Pekka Kinnunen, Weston Anderson, Deepak Ray, Michael J. Puma, Olli Varis, Stefan Siebert, Matti Kummu

Corresponding authors: Matias Heino, Matti Kummu
Emails: matias.heino@aalto.fi, matti.kummu@aalto.fi

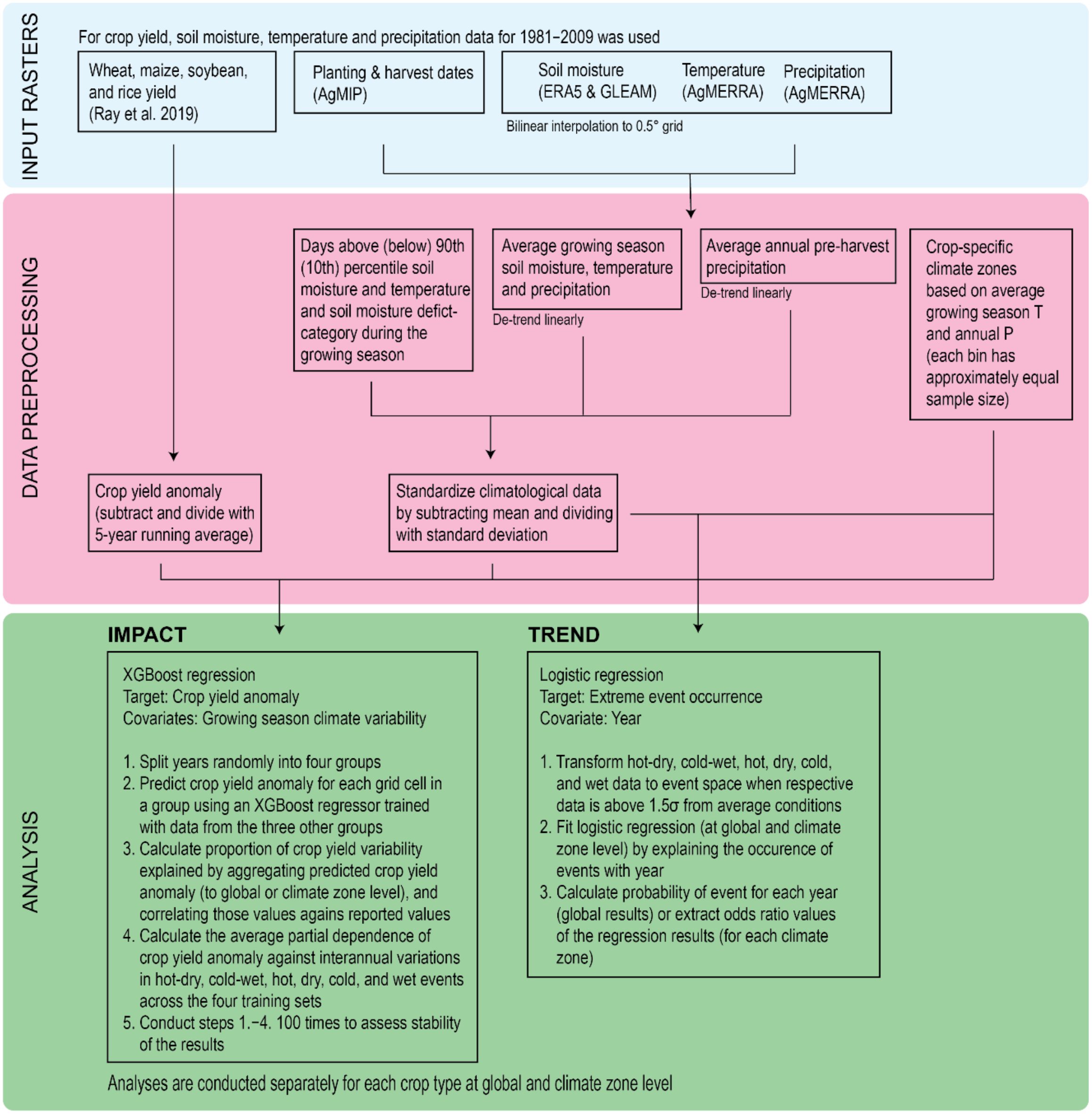

Fig. S1. Methodological framework of the study.

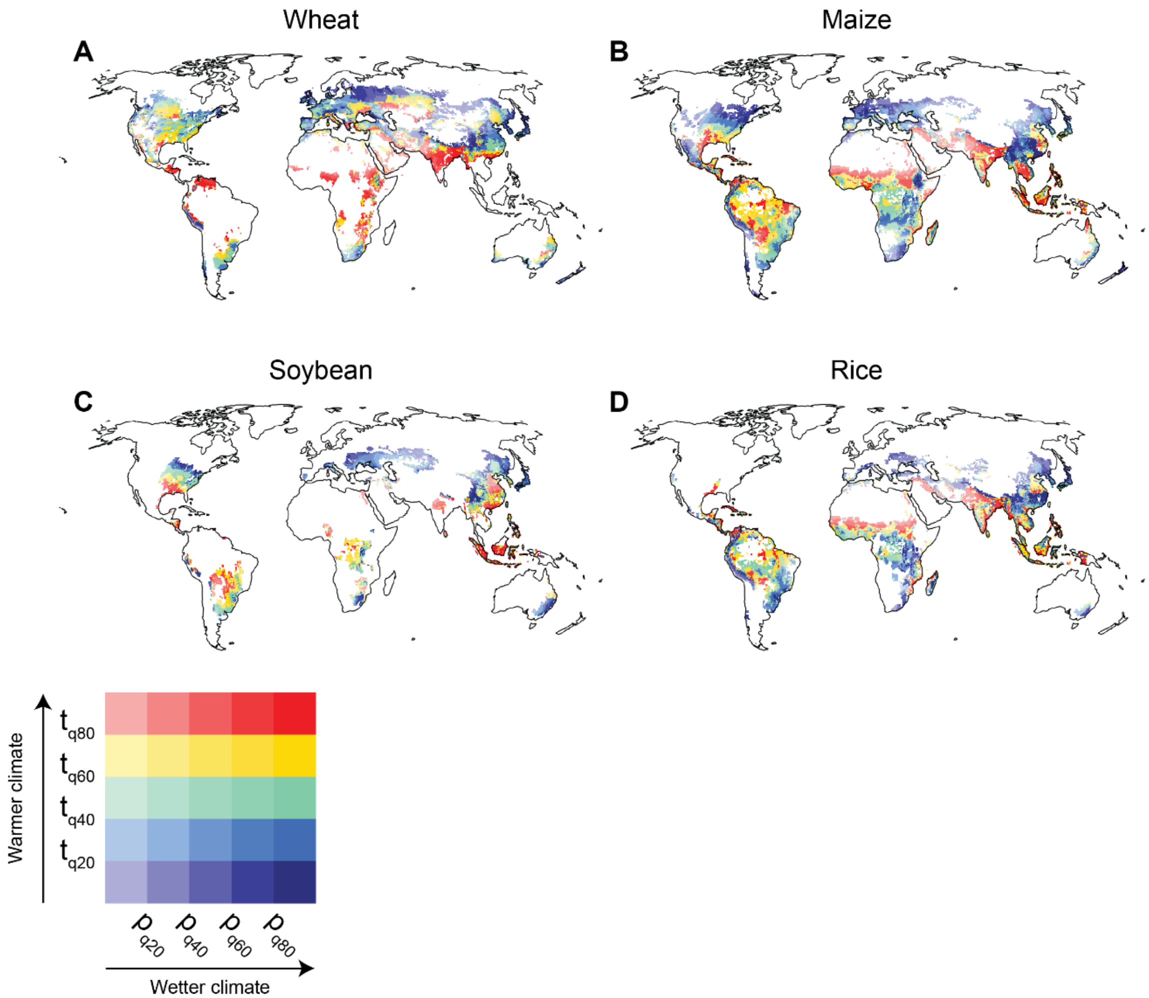

Fig. S2. Crop-specific climate zones for wheat (A), maize (B), soybean (C), and rice (D). The zoning is based on growing season average temperature and annual precipitation (1). For each crop, the zoning was conducted in two steps. First, all considered grid cells were divided into quintiles based on growing season temperature. After that, each temperature quintile was again divided into quintiles based on annual precipitation.

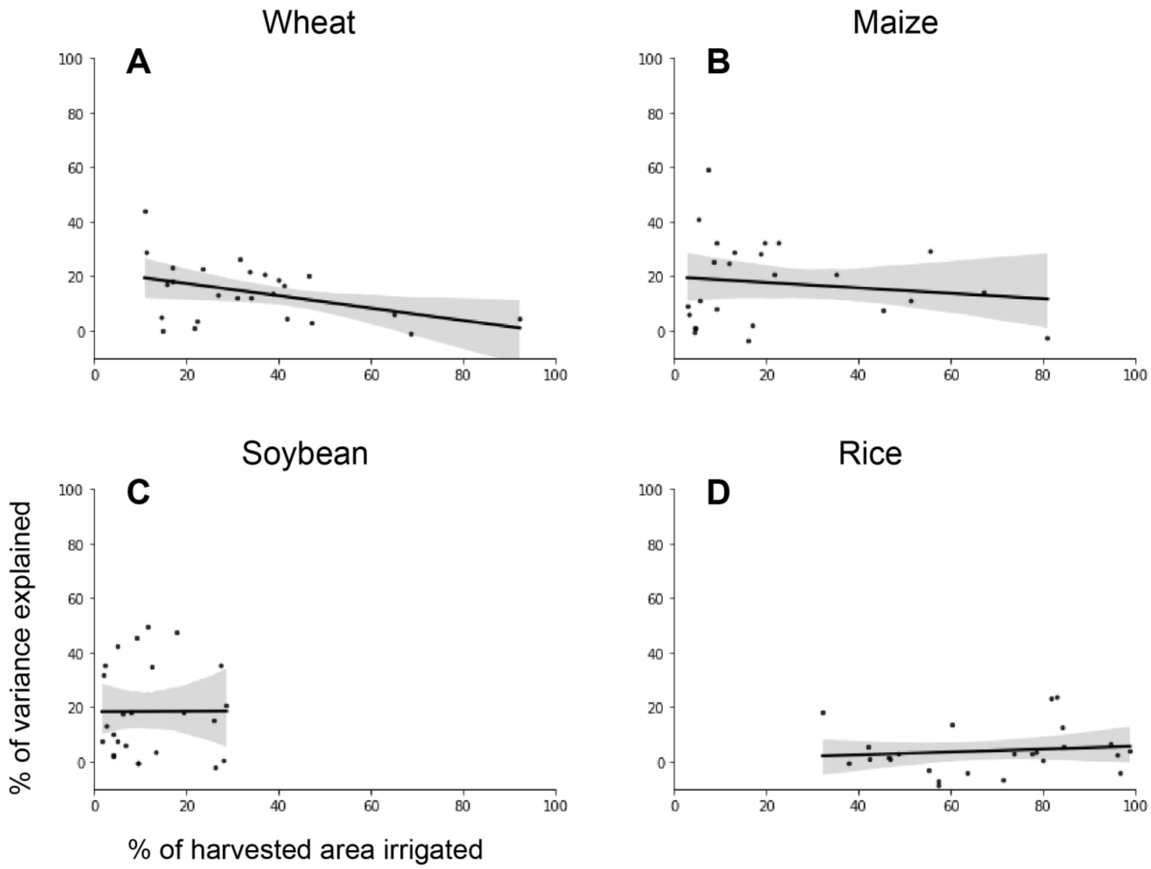

Fig. S3. The relationship between proportion of irrigated areas (2) and proportion of wheat (A), maize (B), soybean (C), and rice (D) yield variance explained by climate variability. Each point represents one climate zone.

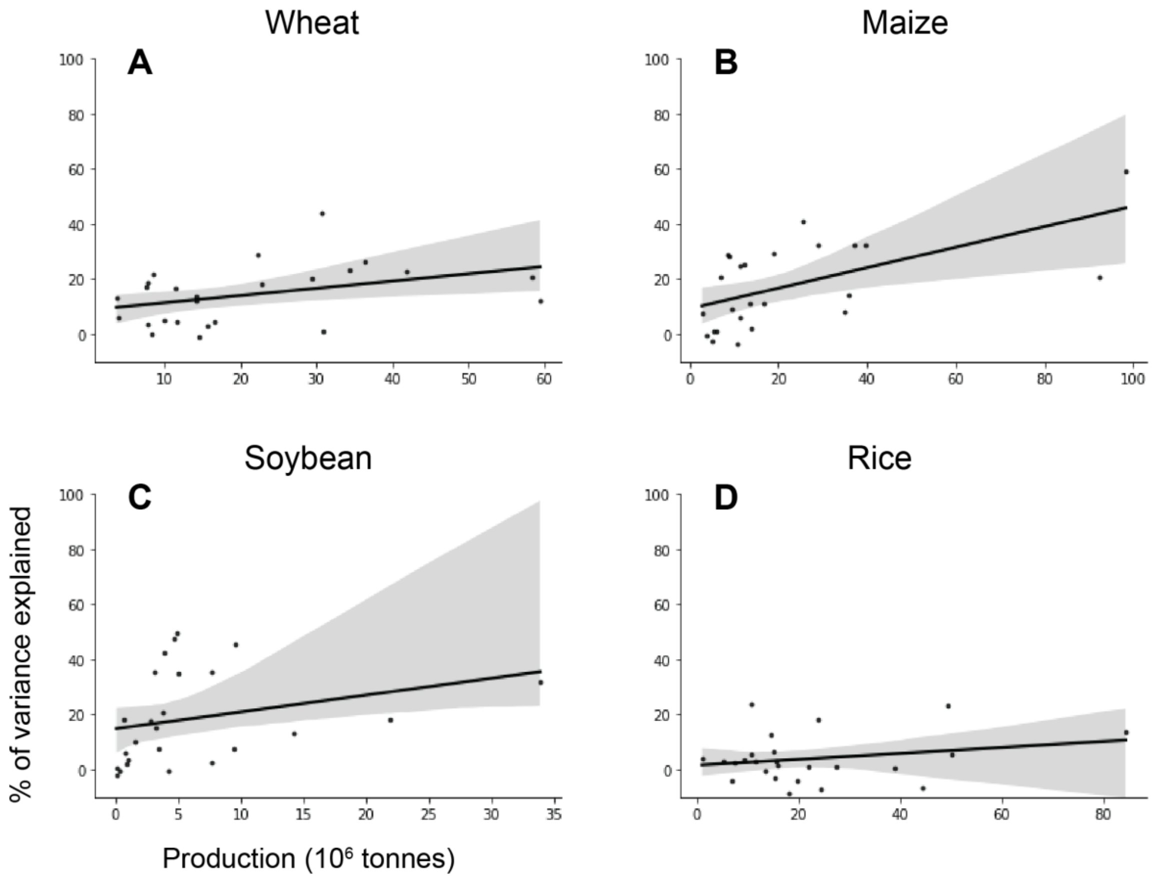

Fig. S4. The relationship between wheat (A), maize (B), soybean (C), and rice (D) production and proportion of their yield variance explained by climate variability. Each point represents one climate zone.

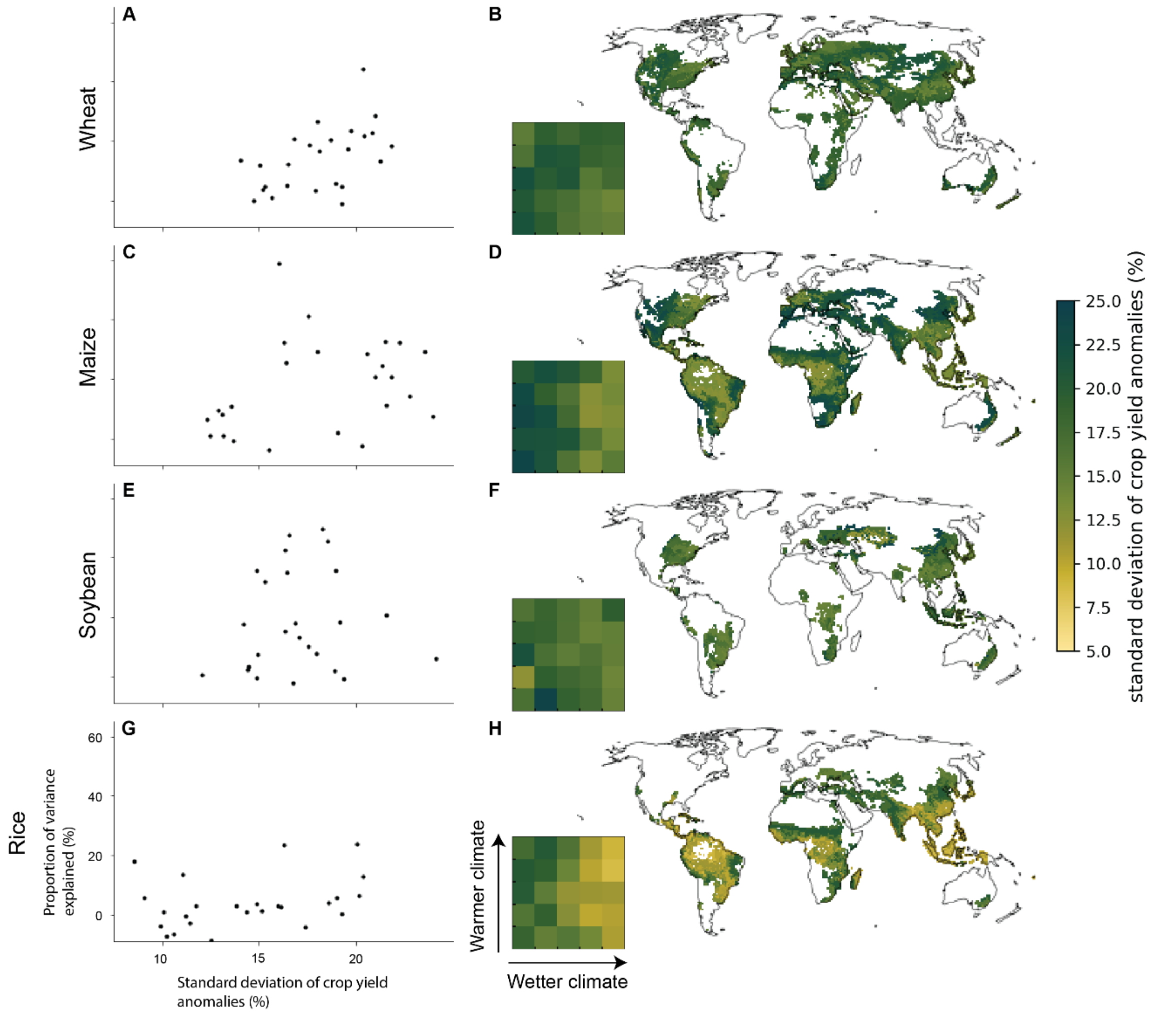

Fig S5. The relationship between wheat (A, B), maize (C, D), soybean (E, F), and rice (G, H) variability and proportion of their yield variance explained by climate variability at climate zone level. In the scatter plot, each point represents one climate zone.

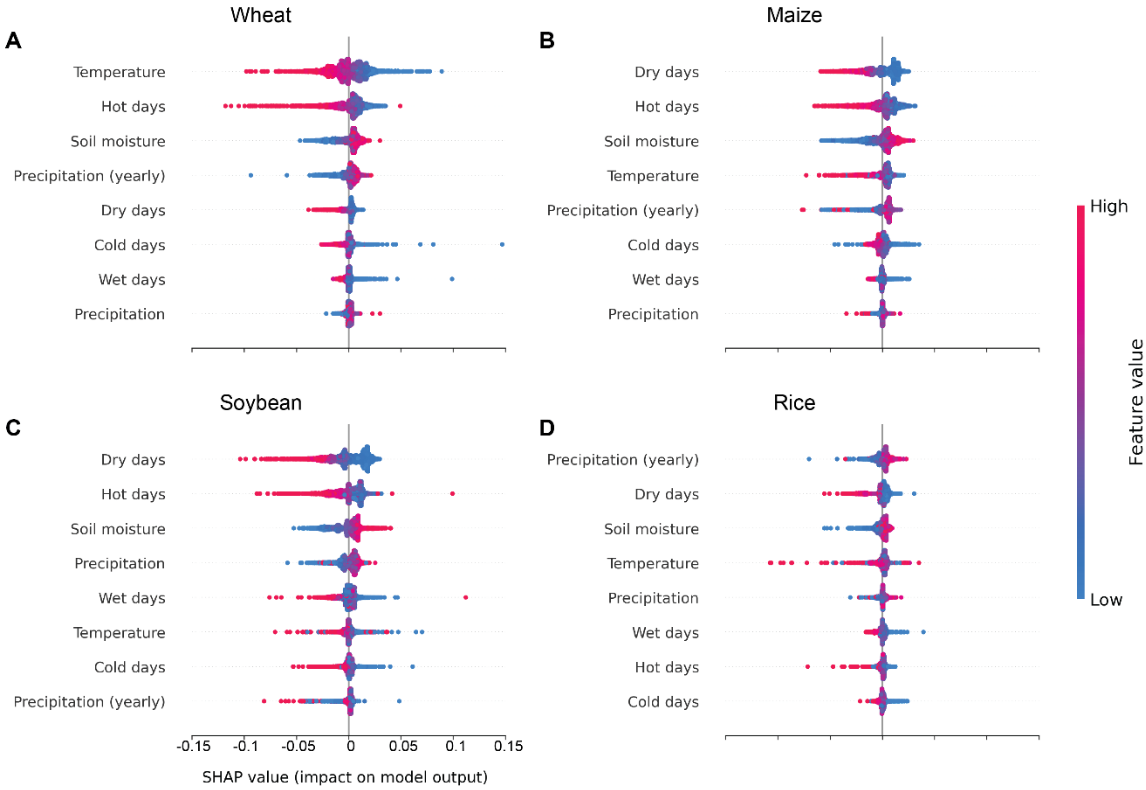

Fig. S6. SHAP summary plots for wheat (A), maize (B), soybean (C), and rice (D) derived from the globally fitted XGBoost regression models of the main analyses. Each point represents the Shapley value, i.e., the contribution of the climatological variable (feature) to the predicted outcome, for an instance of the data (3). The climatological variables are ordered by their importance in the predictions, the top variable being the most important.

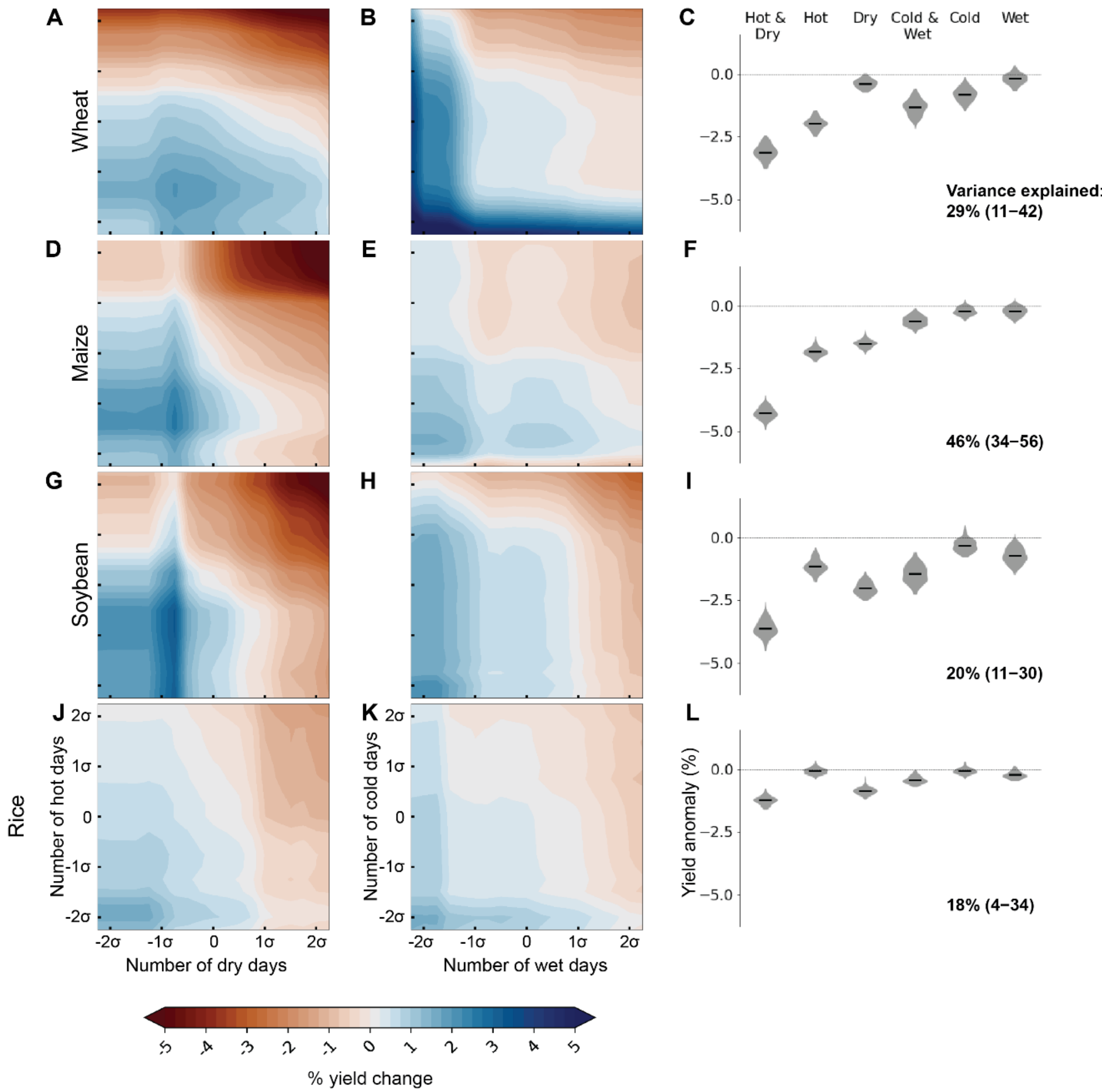

Fig. S7. Same as Figure 2, but with GLEAM (4) soil moisture data.

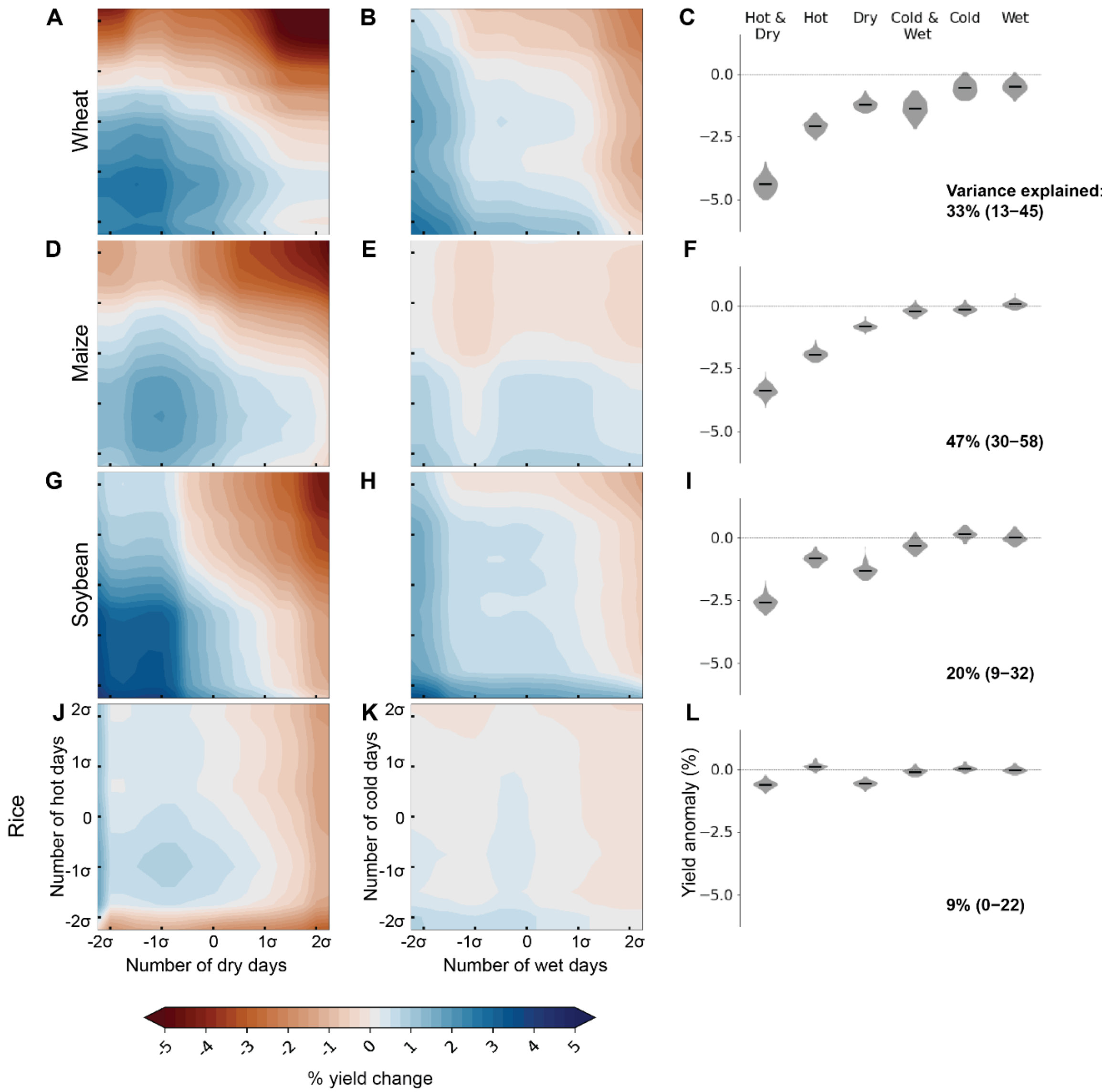

Fig. S8. Same as Figure 2, but with extreme indicators (i.e., anomaly in hot, dry, cold, and wet days during the growing season) also linearly de-trended.

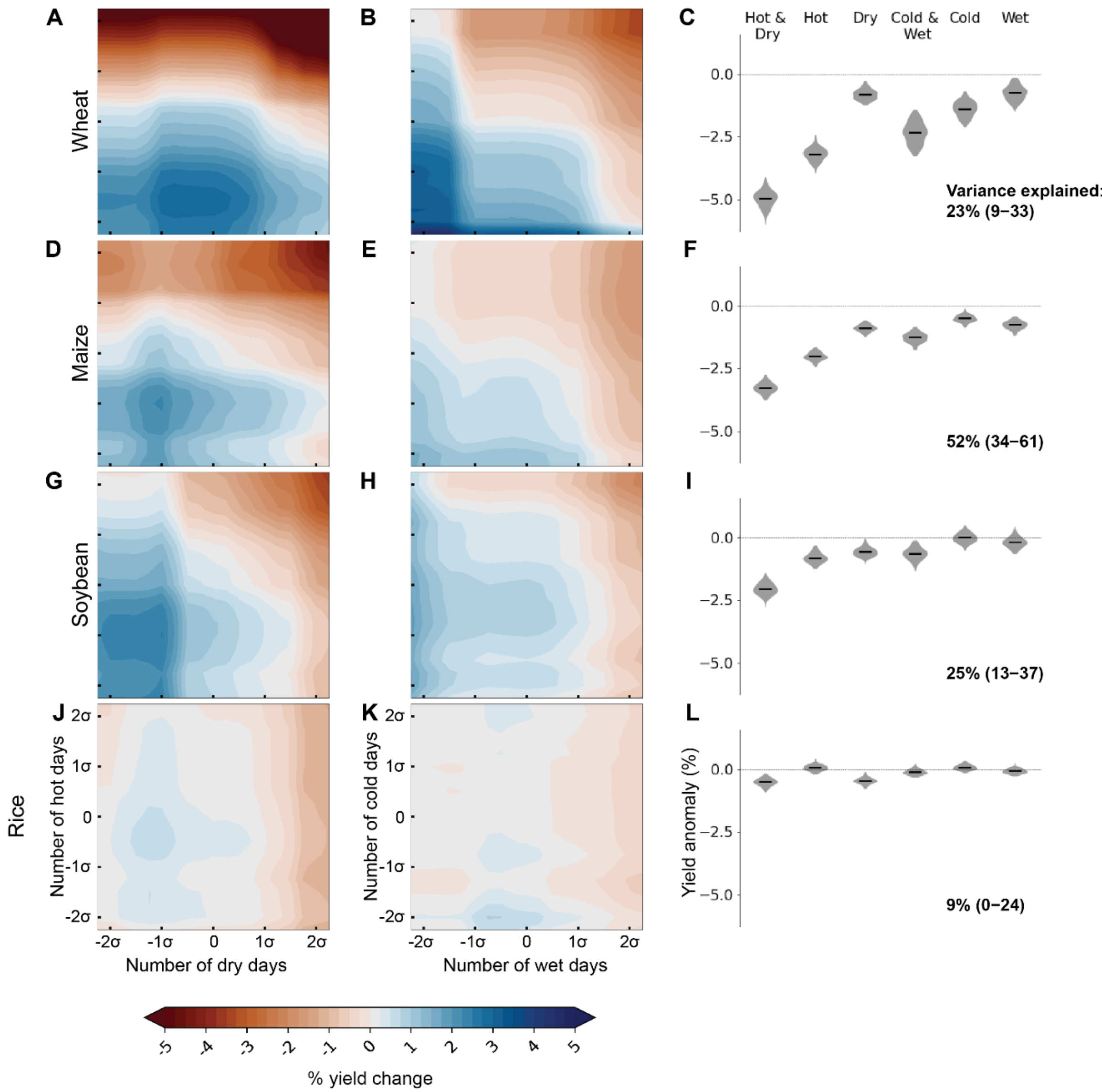

Fig. S9. Same as Figure 2, but with full growing season (5) climate data.

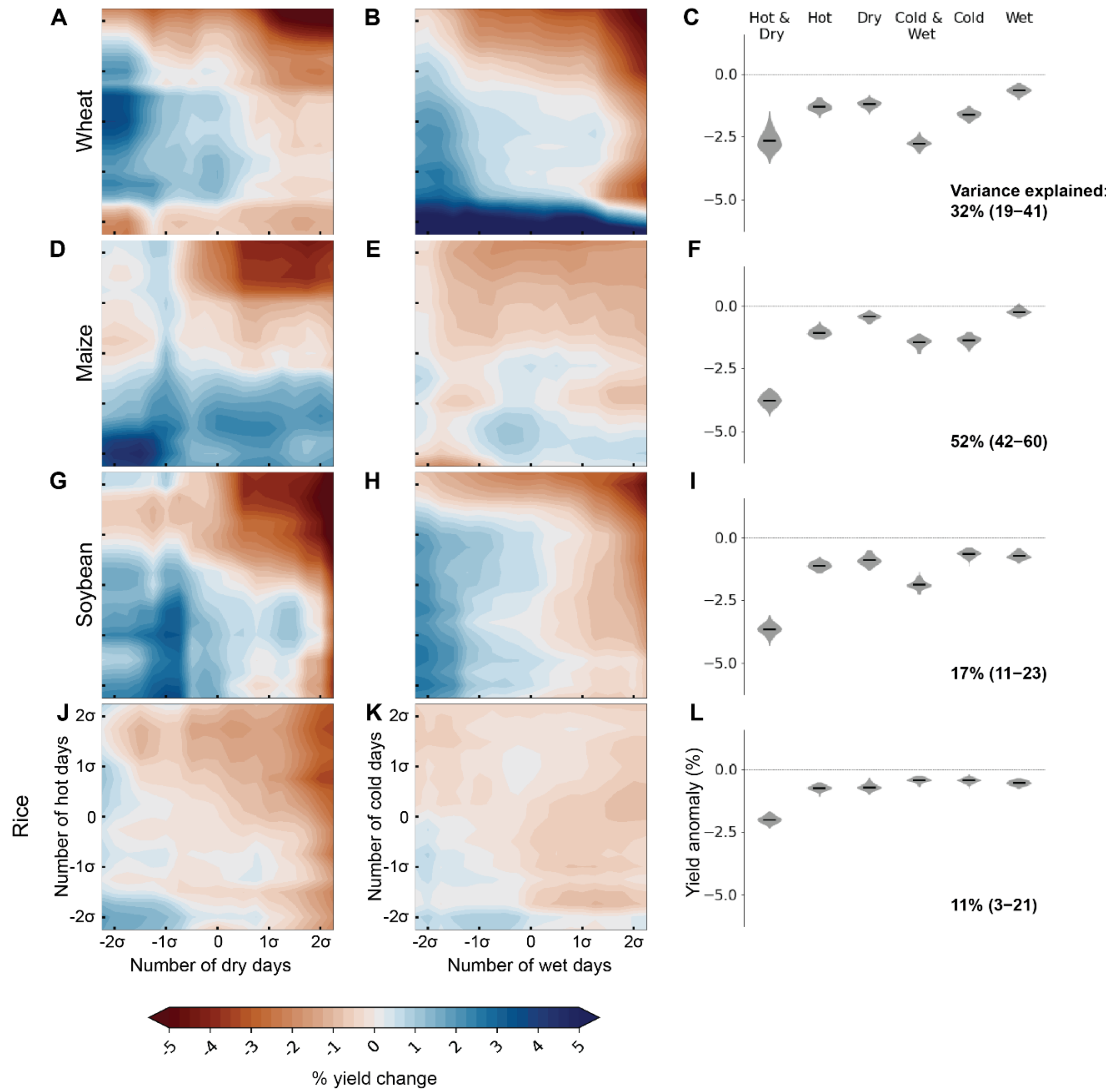

Fig. S10. Same as Figure 2, but with a Random Forest model (6). Here, Random Forest is trained with 50 trees so that in each tree, the nodes are expanded until all leaves are pure.

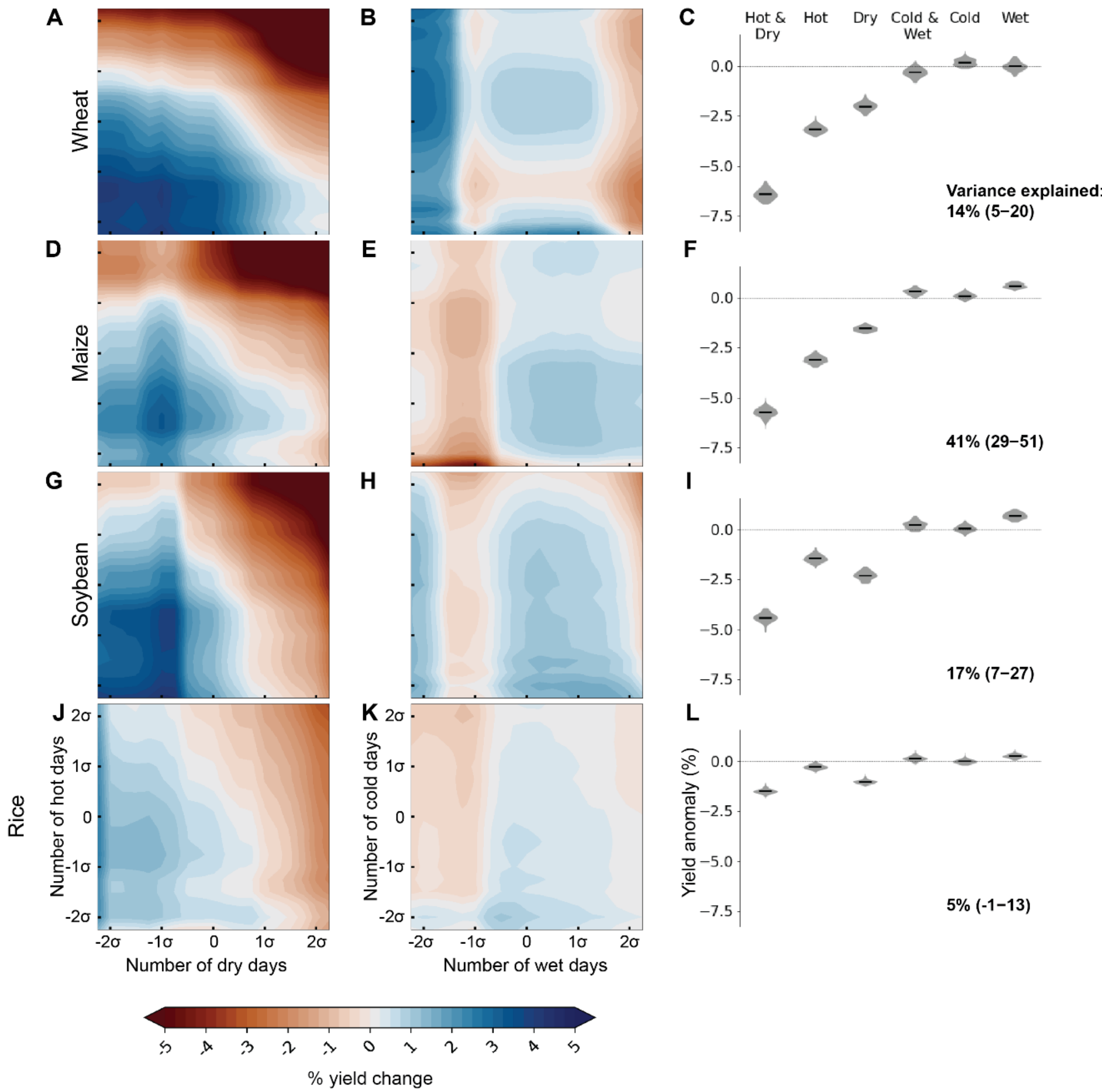

Fig. S11. Same as Figure 2, but with solely the number of hot, dry, wet, and cold days as explanatory variables.

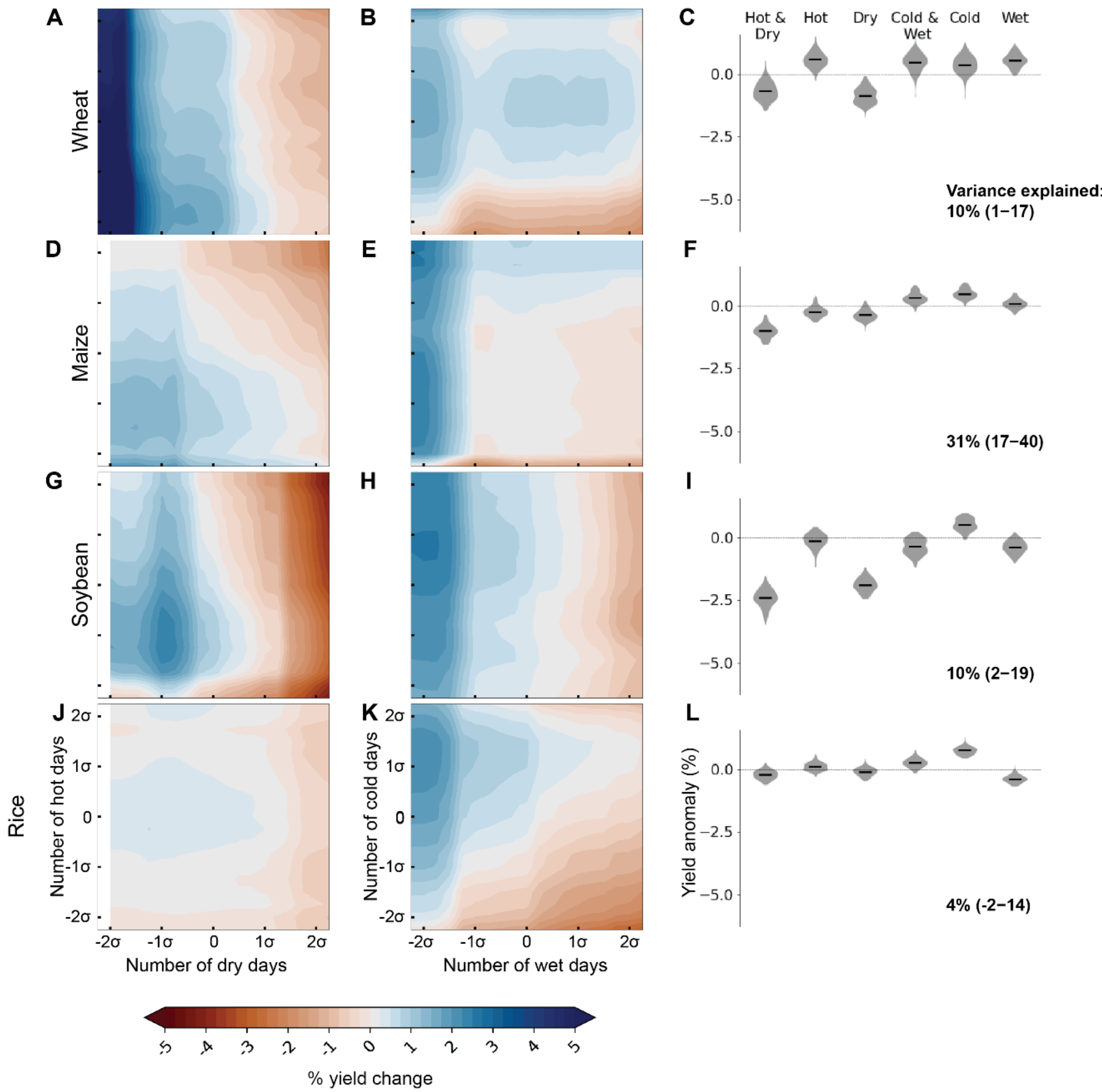

Fig S12. Same as Figure 2, but with Iizumi et al. (2020) (7) crop yield data.

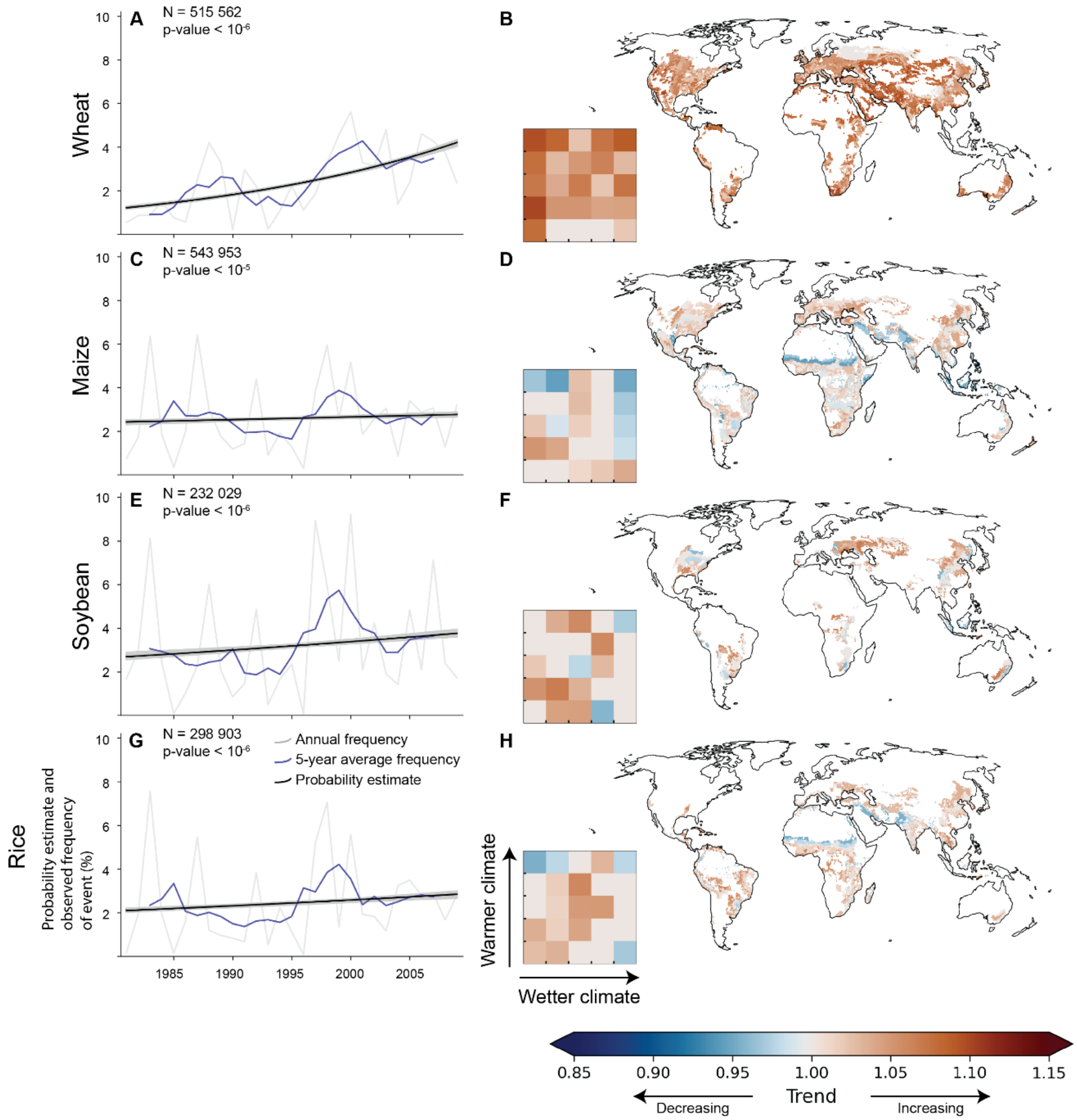

Fig. S13. Same as Figure 4, but for GLEAM (4) soil moisture data.

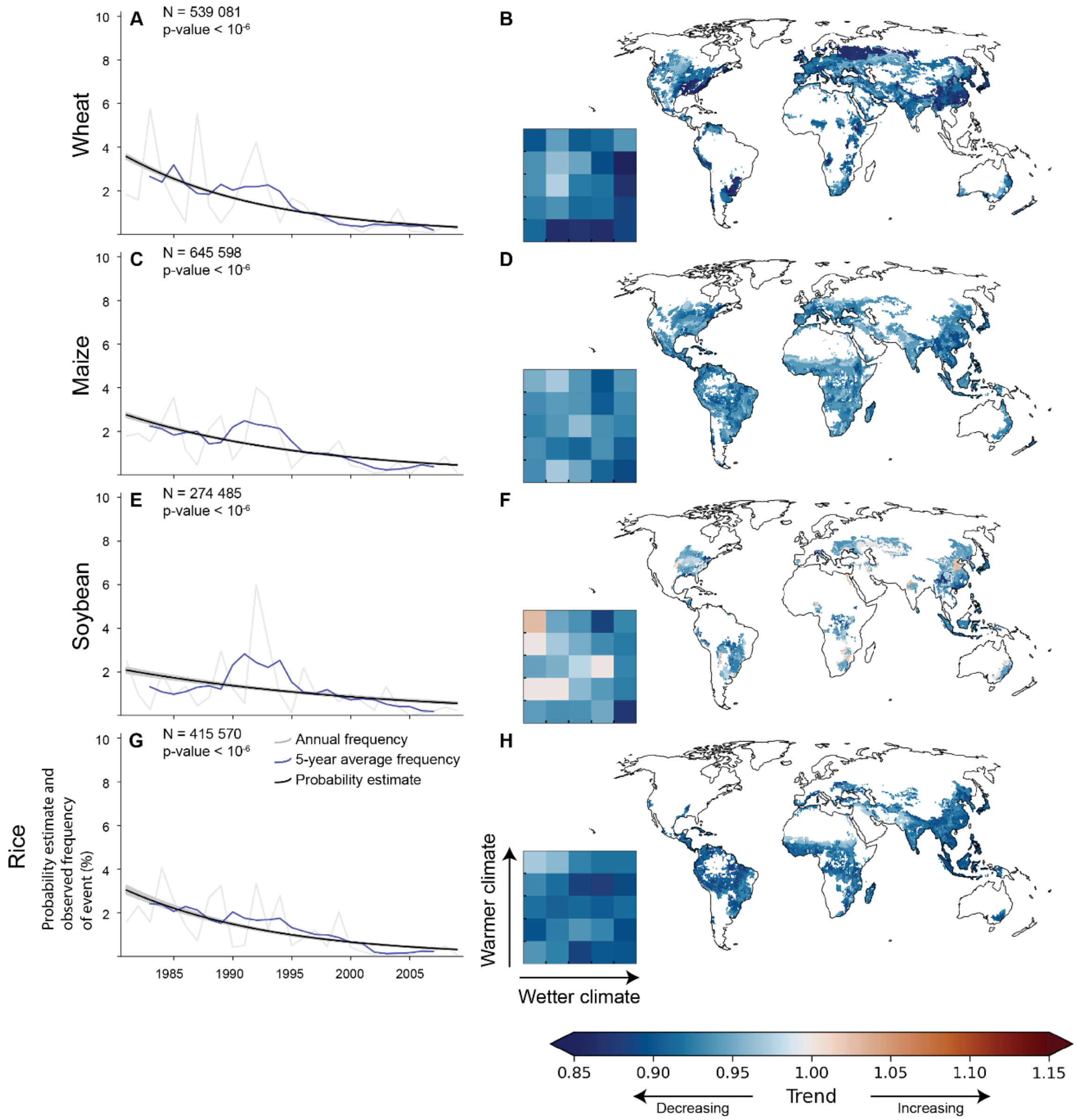

Fig. S14. Same as Figure 4, but for wet and cold events.

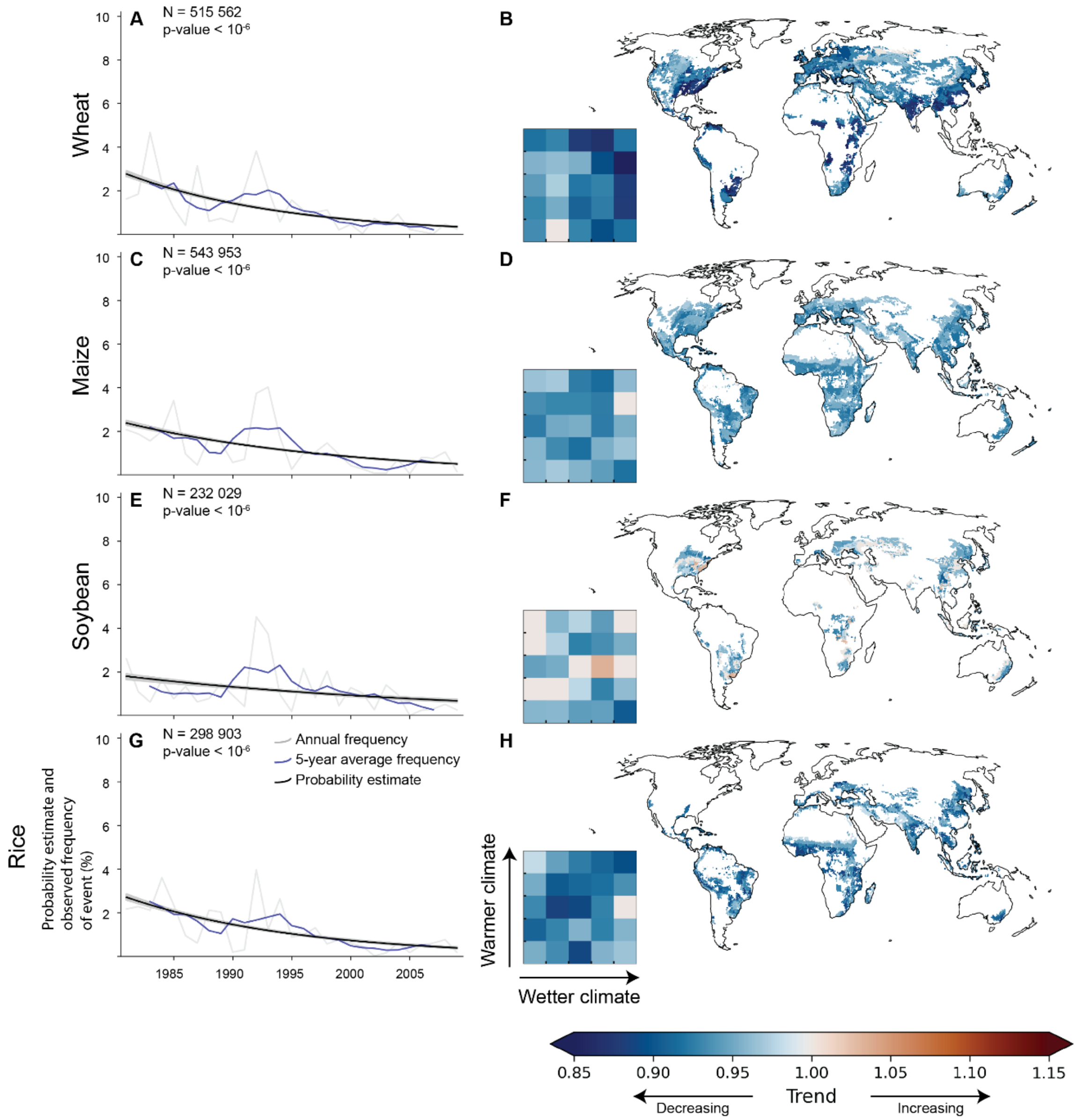

Fig. S15. Same as Figure 4, but for wet and cold events and GLEAM (4) soil moisture data.

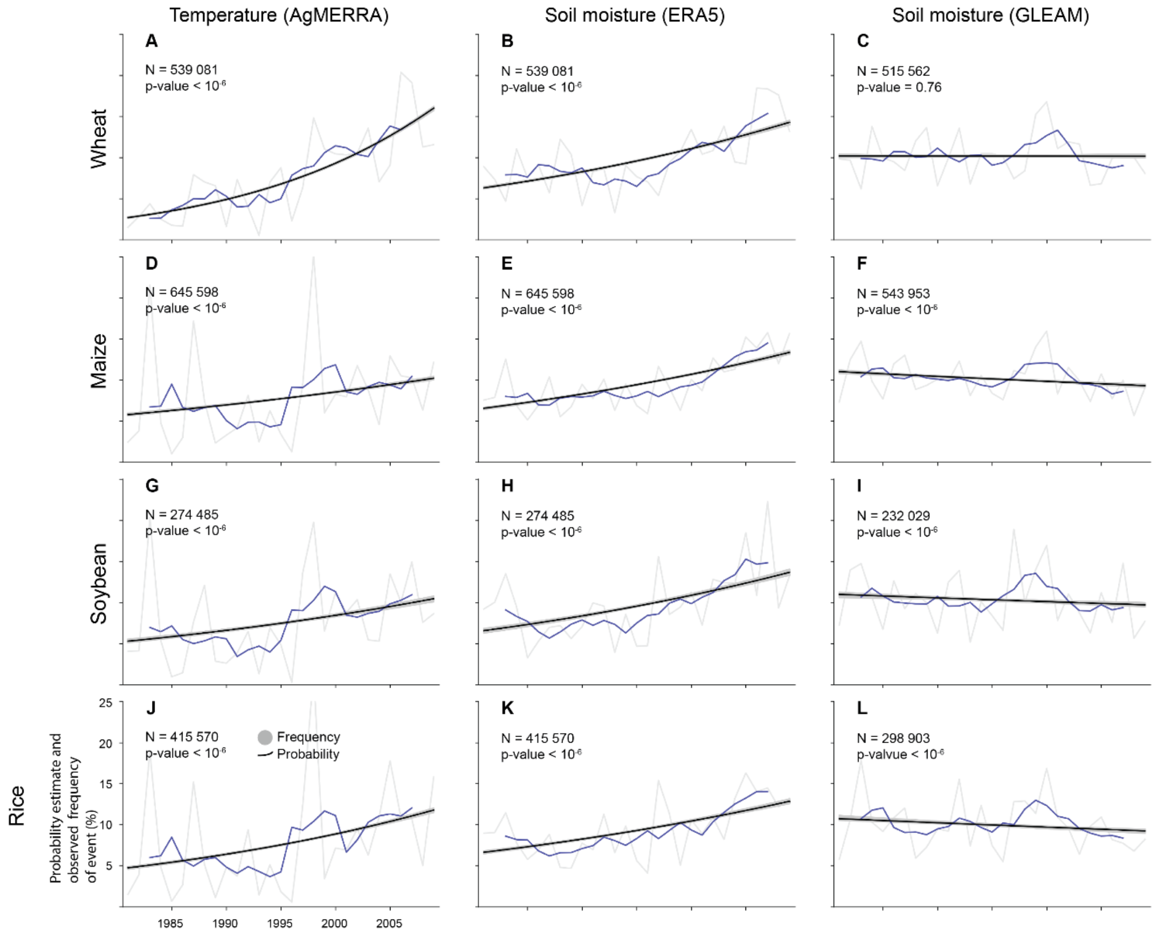

Fig. S16. Historical evolution in the probability of hot (1) and dry (4, 8) conditions between 1980–2009. Results are shown for studied crops: wheat (A,B,C), maize (D,E,F), soybean (G,H,I), and rice (J,K,L). The analysis was conducted utilizing data for all raster cells across the globe with both crop yield and weather data for the respective crop types. Here, a grid cell is considered hot (dry) for a specific year, if the number hot (dry) days during the growing season deviates at least 1.5σ from the long-term average. The historical evolution of the probability in hot (dry) events was assessed by logistic regression, while frequency was calculated as a percentage of hot (dry) events for each year and as a five-year average. The uncertainty intervals for the regression lines in the figure were calculated by bootstrapping (N=100) the observations and plotting the regression line for each sample (in gray color).

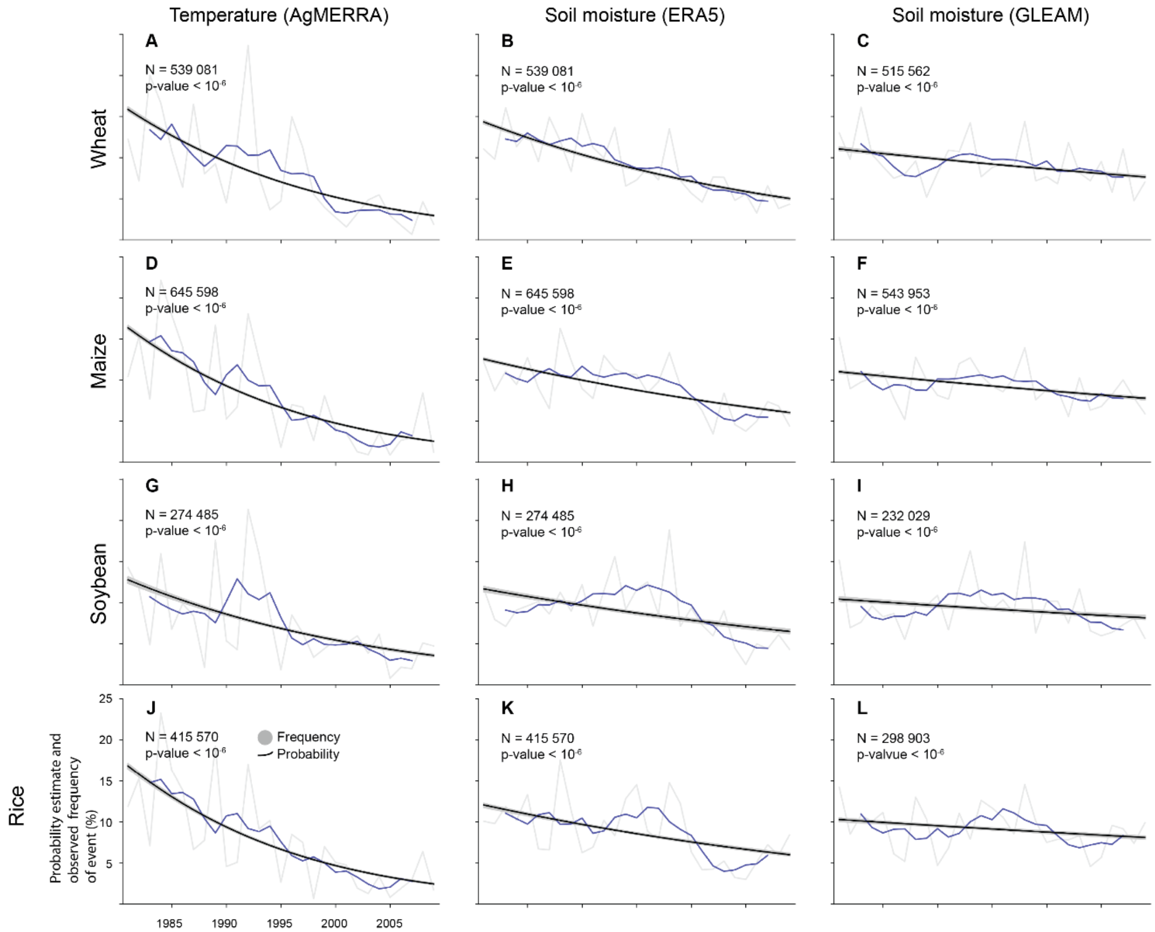

Fig. S17. Historical evolution in the probability of cold (1) and wet (4, 8) conditions between 1980–2009. Results are shown for studied crops: wheat (A,B,C), maize (D,E,F), soybean (G,H,I), and rice (J,K,L). The analysis was conducted utilizing data for all raster cells across the globe with both crop yield and weather data for the respective crop types. Here, a grid cell is considered cold (wet) for a specific year, if the number cold (wet) days during the growing season deviates at least 1.5σ from the long-term average. The historical evolution of the probability in cold (wet) events was assessed by logistic regression, while frequency was calculated as a percentage of cold (wet) events for each year and as a five-year average. The uncertainty intervals for the regression lines in the figure were calculated by bootstrapping (N=100) the observations and plotting the regression line for each sample (in gray color).

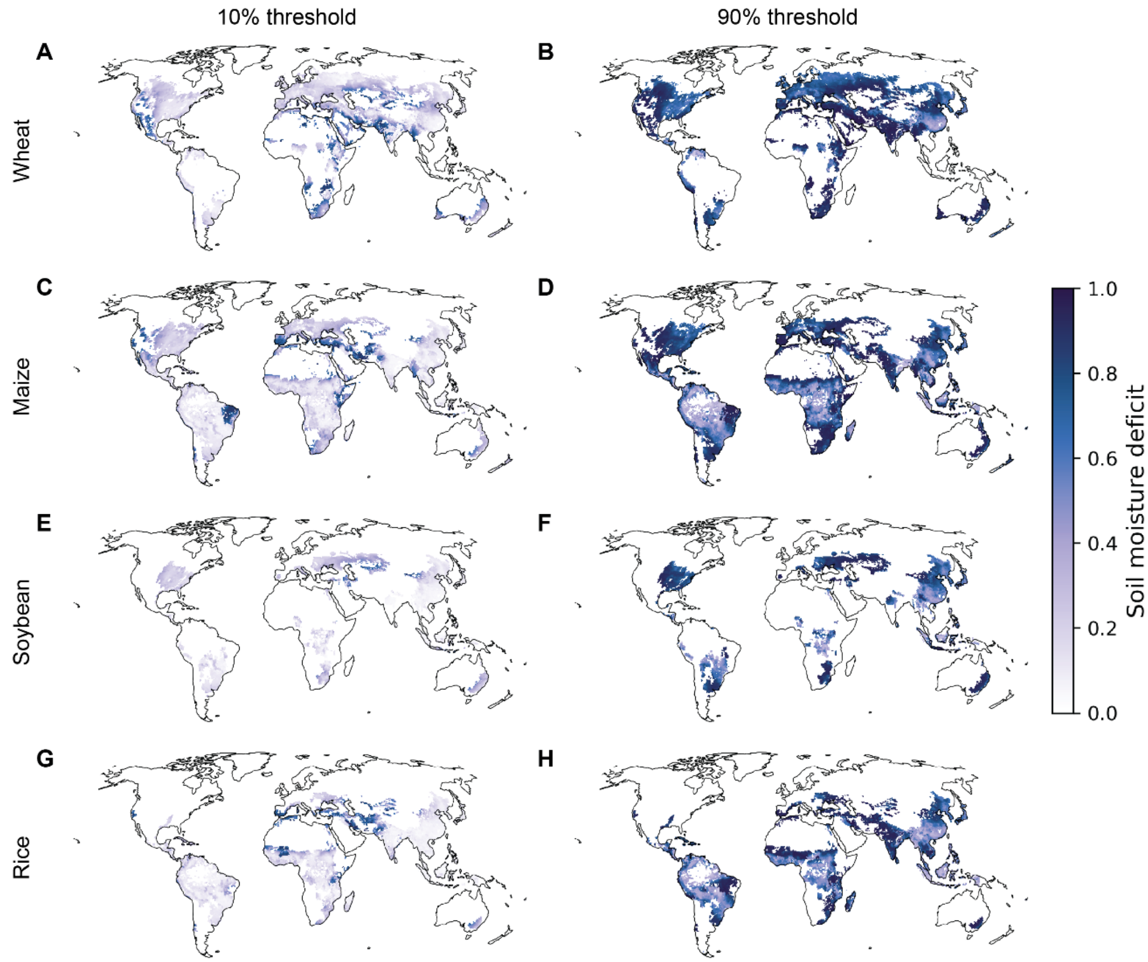

Fig. S18. 10% (A,C,E,G) and 90% (B,D,F,H) percentiles for soil moisture deficit (derived from ERA5 (8)) for each raster cell during wheat (A,B), maize (C,D), soybean (E,F), and rice (G,H) growing seasons.

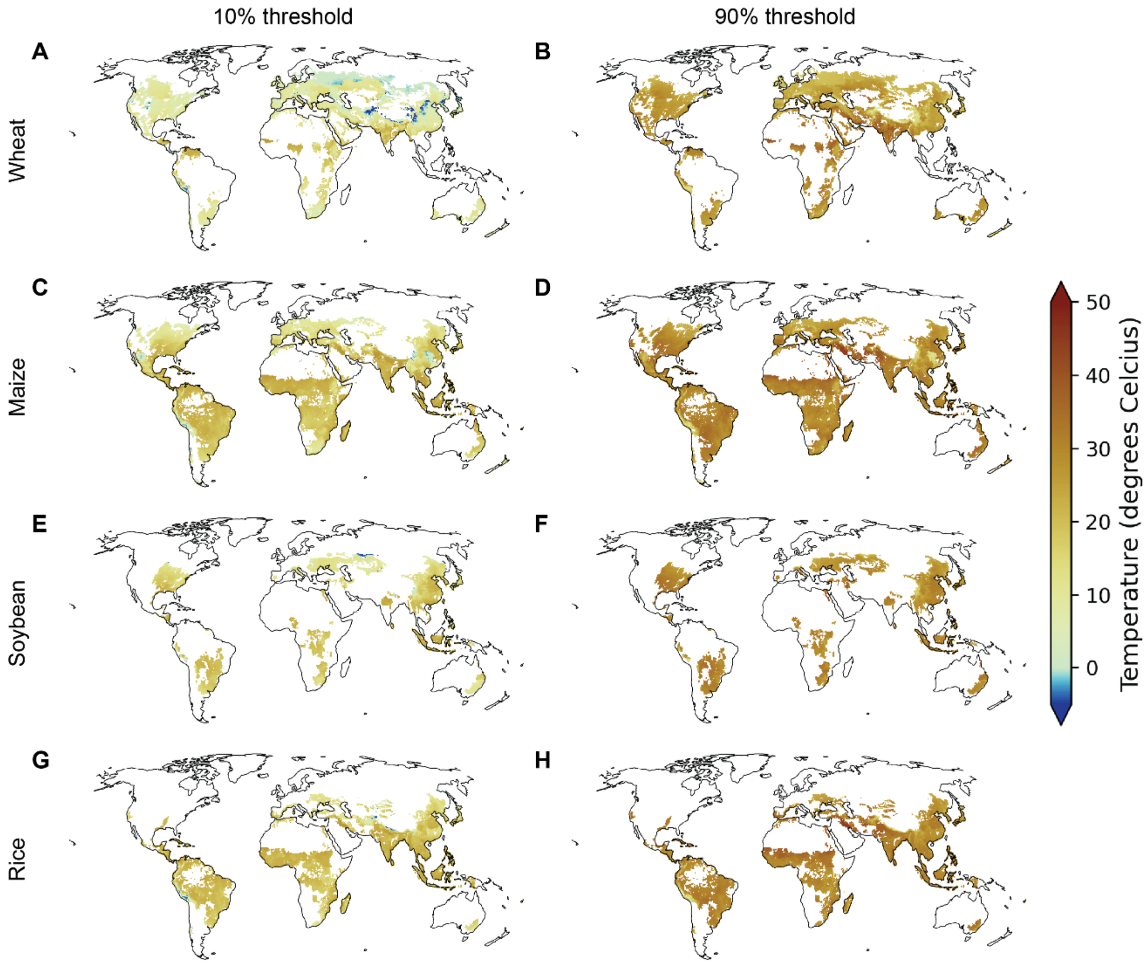

Fig. S19. 10% (A,C,E,G) and 90% (B,D,F,H) percentiles for temperature (1) for each raster cell during wheat (A,B), maize (C,D), soybean (E,F), and rice (G,H) growing seasons.

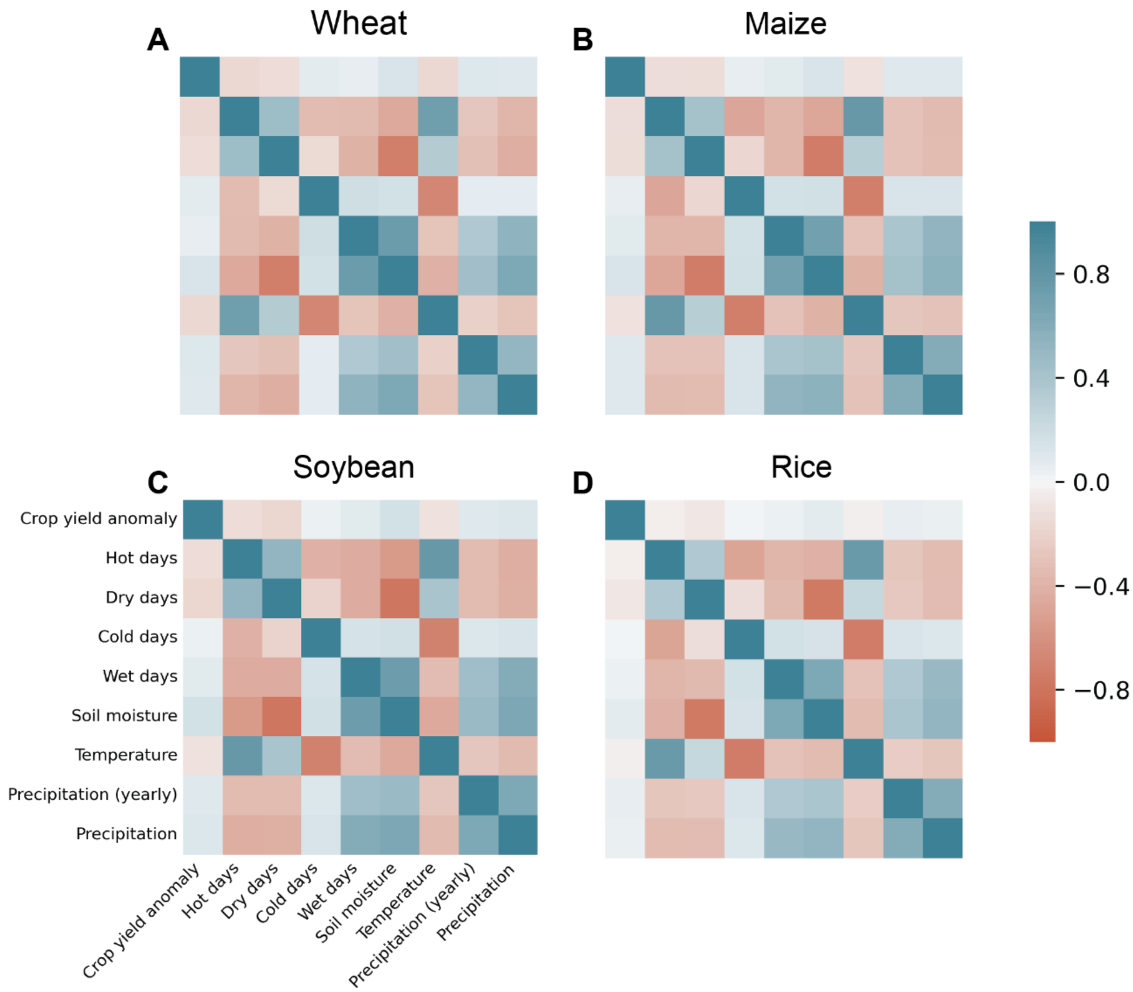

Fig. S20. Pearson's correlation matrices of yield anomalies and the growing season climate variables indicators for wheat (A), maize (B), soybean (C), and rice (D) across all grid cells included in the global regression analyses conducted with the Ray et al. (2019) crop yield data (9).

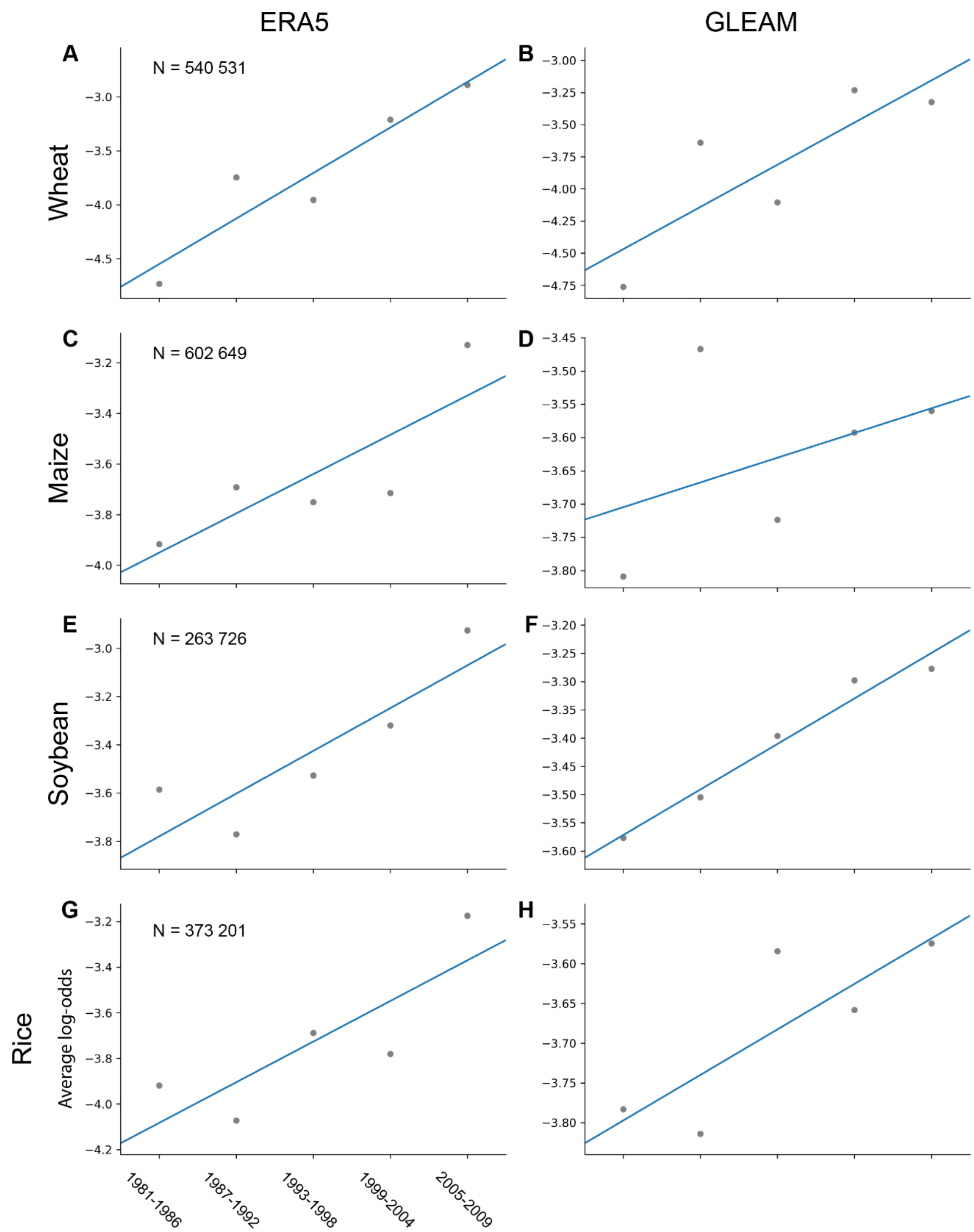

Fig. S21. Average log-odds values of co-occurring dry and hot events for each temporally defined quintile with ERA5 (8) and GLEAM (10) soil moisture data. Results are shown for studied crops: wheat (A,B), maize (C,D), soybean (E,F), and rice (G,H).

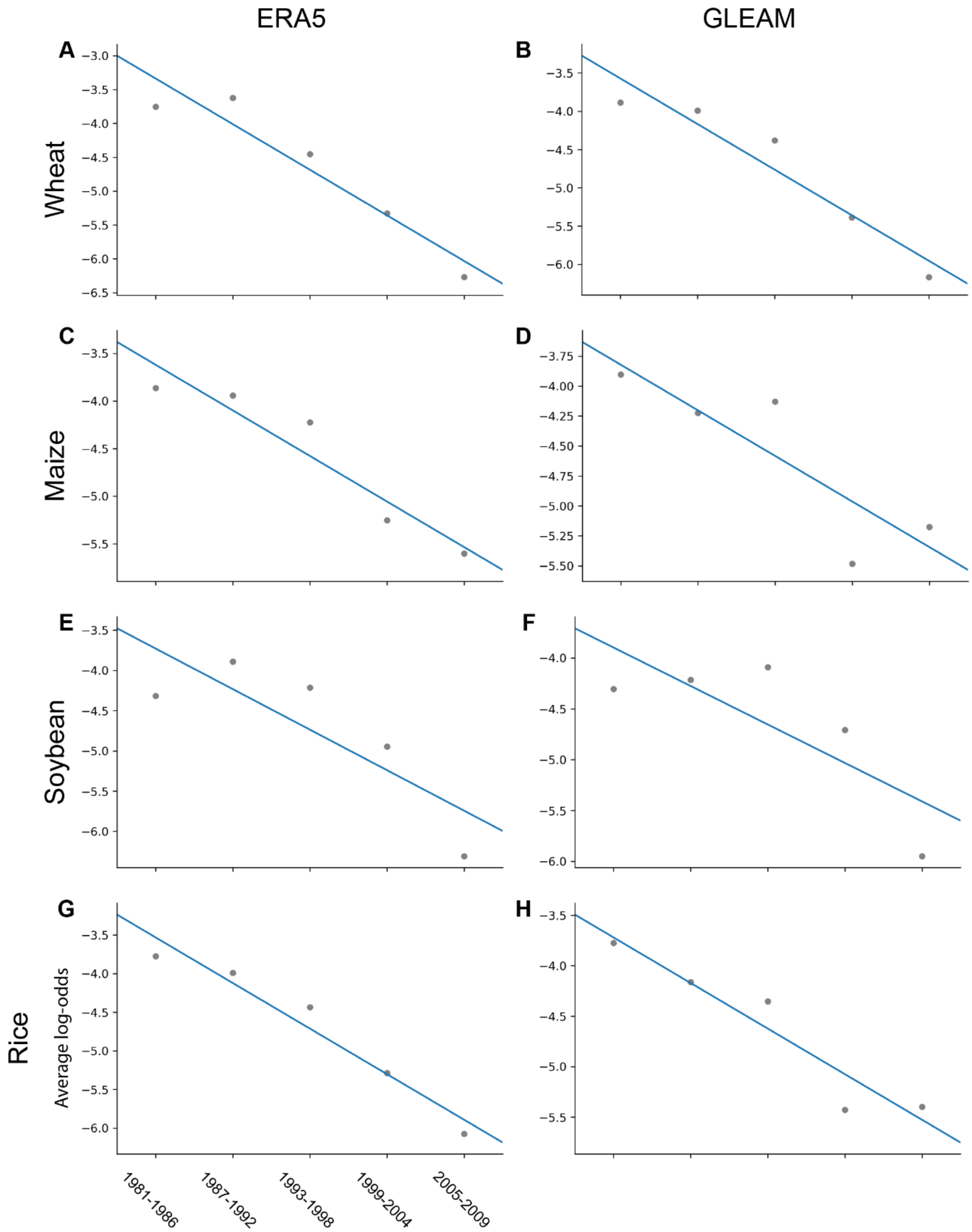

Fig. S22. Average log-odds values of co-occurring cold and wet events for each temporally defined quintile with ERA5 (8) and GLEAM (10) soil moisture data. Results are shown for studied crops: wheat (A,B), maize (C,D), soybean (E,F), and rice (G,H).

SI References

1. Ruane AC, Goldberg R & Chryssanthacopoulos J (2015) Climate forcing datasets for agricultural modeling: Merged products for gap-filling and historical climate series estimation. *Agric for Meterol* 200: 233-248.

2. Portmann FT, Siebert S & Döll P (2010) MIRCA2000—Global monthly irrigated and rainfed crop areas around the year 2000: A new high-resolution data set for agricultural and hydrological modeling. *Global Biogeochem Cycles* 24(1)

3. Lundberg SM, *et al* (2020) From local explanations to global understanding with explainable AI for trees. *Nature Machine Intelligence* 2(1): 56-67.

4. Martens B, *et al* (2017) GLEAM v3: Satellite-based land evaporation and root-zone soil moisture. *Geoscientific Model Dev* 10(5): 1903-1925.

5. Müller C, *et al* (2017) Global gridded crop model evaluation: Benchmarking, skills, deficiencies and implications. *Geoscientific Model Dev* 10(4): 1403-1422.

6. Breiman L (2001) Random forests. *Mach Learn* 45(1): 5-32.

7. Iizumi T & Sakai T (2020) The global dataset of historical yields for major crops 1981–2016. *Sci Data* 7(1)

8. Hersbach H, *et al* (2020) The ERA5 global reanalysis. *Q J R Meteorol Soc*

9. Ray DK, *et al* (2019) Climate change has likely already affected global food production. *PLoS ONE* 14(5)

10. Martens B, *et al* (2017) GLEAM v3: Satellite-based land evaporation and root-zone soil moisture. *Geoscientific Model Dev* 10(5): 1903-1925.